


Research Article

Internal Model Control (IMC)-Based Active and Reactive Power Control of Brushless Double-Fed Induction Generator with Notch Filter

Ahsanullah Memon ^{1,2}, Mohd Wazir Bin Mustafa,¹ Zohaib Hussain Laghari,³ Touqeer Ahmed Jumani,² Waqas Anjum,⁴ Shafi Ullah,⁵ and Muhammad Naveed Aman⁶

¹Department of Electrical Power Engineering, Faculty Engineering, Universiti Teknologi Malaysia (UTM), Skudai 81310, Johor, Malaysia

²Department of Electrical Engineering, Mehran University of Engineering and Technology, SZAB Campus, Khairpur Mir's, Sindh, Pakistan

³Department of Electrical Engineering, Mehran University of Engineering and Technology, Jamshoro, Sindh, Pakistan

⁴Department of Electronic Engineering, The Islamia University of Bahawalpur, Bahawalpur, Pakistan

⁵Department of Computer Engineering, BUIITEMS, Quetta 87300, Pakistan

⁶Department of Computer Science and Engineering, University of Nebraska-Lincoln, Lincoln, NE, USA

Correspondence should be addressed to Ahsanullah Memon; memon.ahsanullah@graduate.utm.my

Received 16 December 2021; Revised 19 April 2022; Accepted 8 June 2022; Published 18 July 2022

Academic Editor: Youssef Errami

Copyright © 2022 Ahsanullah Memon et al. This is an open access article distributed under the Creative Commons Attribution License, which permits unrestricted use, distribution, and reproduction in any medium, provided the original work is properly cited.

The increase in demand for electricity and, in particular, green energy has put renewable energy systems at the focal point of energy policy worldwide. The higher reliability of brushless doubly fed induction generators (BDFIGs) makes them suitable for offshore and remote wind energy generation (WEG) applications. Besides, controlling the active and reactive powers in an electrical power system is critical for optimal voltage regulation, reduced power losses, and enhanced utilization of installed equipment. However, the existing literature on BDFIG's active and reactive power control highlights the poor dynamic response and high transients with harmonic generation during inductive load insertion. It is because the Ziegler technique was employed to select PI gains, and the instantaneous reactive power theory was used to mitigate harmonics. Considering that, this paper proposes a vector control (VC) method for BDFIGs in wind turbines, in which the proportional-integral (PI) gains for internal model control (IMC) are optimized to improve the dynamic response of the active and reactive power during inductive load insertion. The proposed method reduces the complexity, time consumption, and uncertainty in making the optimal choice. In addition, to reduce a double fundamental frequency component to the point-of-common-coupling (PCC) voltage, the excellent characteristics of the notch filter are utilized in the grid-side converter (GSC)-based vector control scheme. The simulation results in MATLAB/Simulink show that the proposed IMC-based vector control scheme with a notch filter provides satisfactory results with a minimum peak value compared to existing techniques.

1. Introduction

As the global demand for electrical energy grows, renewable energy systems (RES) have become increasingly popular because of their eco-friendly nature [1]. Over the past decade, wind energy generation systems (WEGs)-based RES have gained considerable popularity for operating at a

variable speed and constant frequency, with a broader range of aerodynamic efficiencies [2]. The doubly fed induction generator (DFIG)-based WEGs contains brush gears that get stuck in remote locations and prove challenging for offshore applications. On the other hand, the brushless double-fed induction generator (BDFIG) does not have brush gear, which is more reliable than the conventional induction

generator [3]. Besides, the BDFIG has a simple structure (since the slip gear is not needed) and a lower cost than a comparable DFIG. It has led the BDFIGs to attract the attention of researchers and industries. A BDFIG consists of two separate sets of three-phase stator windings [4]. The stator winding connected with the grid is called the power winding (PW) and is responsible for generating electrical power. The second stator winding, called the control winding (CW), is indirectly connected to the grid through a fractionally rated converter. The rotor is used to couple the two stator windings [5], whereas the pole pairs are different on each stator to avoid direct coupling between the two stator windings.

As part of the BDFIG control scheme, one of the primary objectives is to enhance the dynamic response, maintain constant power, and mitigate harmonics in the presence of loads [6]. In literature, researchers have attempted to control the BDFIG through different techniques that include model predictive virtual torque [7], power control [8], direct power controller (DPC) [9], and stator with indirect control quantities [10]. These methods cannot offer an ideal control over the active and reactive powers with a suitable dynamic response. For this reason, the authors adopted one of the most prominent control schemes, termed vector control (VC) [11, 12], which utilizes four PI regulators in its control structure to tackle the aforementioned problem.

This study uses the internal model control (IMC) approach to efficiently tune the PI regulators, leading to an optimal dynamic response of the proposed BDFIG. The proposed method eliminates the time constraints and complexity associated with conventional tuning approaches such as the trial and error and Ziegler–Nichols method [13, 14]. The IMC is a way of selecting PI parameters analytically, which considers the system parameters based on the open-loop poles of the PI controller to equalize them with the zeros in order to provide the desired closed-loop bandwidth and time constant [15]. Nonetheless, it simplifies the control design procedure and eliminates the need for time-consuming and inefficient trial and error testing that may be necessary [16]. The dynamic response of the proposed method is evaluated under inductive load conditions to demonstrate its efficacy. Further, it has been demonstrated that the voltage at the point of common coupling (PCC) was susceptible to fluctuation when the load variation was substantial, which affected the other loads connected to the PCC and caused torque pulsations. Besides, due to a power quality problem, voltage variations adversely affect both the generation and a variety of loads using electrical energy.

In addition, the BDFIG is controlled via a rotor-side converter (RSC) or grid-side converter (GSC) in the VC scheme. These power electronic converters utilize the pulse width modulators and become the source of harmonics generation [17]. Besides, the nonlinear loads are also a major cause of harmonic generation in electrical power systems. These harmonic currents are the main threat to the power system as they cause voltage stresses, low power factor, voltage drops, and increased heating in conductors at the PCC [18]. The active and passive filters have been used to

remedy the above problem, but these are not preferred because of their large size, aging, and complexity of tuning. Another most common solution for the harmonic compensation is the use of inductance-capacitance-inductance (LCL) filters with power electronics converters. However, due to the LCL filters, the power system faces stability issues as the resonance region amplifies the unwanted harmonics [19, 20]. Furthermore, many authors have used filters based on a certain theory to mitigate the harmonics. The most prominent theory is the IRP p - q theory which is widely applied in three-phase systems to compensate for the harmonics caused due to nonlinear loads [21, 22]. Since the mentioned theory possesses the transformation method that increases the system's complexity, the system becomes unable to reject the narrowband frequency, ultimately resulting in suboptimal performance. Considering the above-raised problems, hence to mitigate the problem of double fundamental frequency components to the PCC voltage, this paper introduces a notch filter designed with a GSC-based VC scheme. The significant contributions of this paper are as follows:

- (i) A GSC-based VC scheme has been proposed to control PCC's active and reactive power during inductive load insertion
- (ii) An IMC-based approach has been adopted to evaluate the PI gains to enhance the dynamic response of the machine
- (iii) A notch filter has been designed to remove harmonics introduced due to inductive load insertion

The literature related to the control of BDFIG under load conditions is presented in Table 1.

This paper is organized as follows: Section 1 provides a literature review, and Section 2 presents the BDFIG architecture. The proposed technique is described in Section 3. In Section 4, the results of the study are discussed. Finally, the paper is concluded in Section 5.

2. BDFIG Architecture

The architecture of the system considered in this paper is shown in Figure 1. The BDFIG has two stator windings, the PW and the CW of the stator, respectively. The two windings of the BDFIG are coupled together by the rotor winding of the BDFIG. Three-phase resistive-inductive RL load is connected to the PW of the stator and the grid (transformer). In a CW of the stator, two voltage source converters are connected back-to-back which are rotor-side converters (RSC) and grid-side converters (GSC). The DC-link is the bridging device between the two converters, which allows for an independent controller design for the RSC and the GSC based on the use of capacitors. The GSC is attached to the stator PW at the point of common coupling (PCC). It should be noted that R_L and L_L are, respectively, the equivalent load resistance and inductance of a load.

To enable VC of the machine, the PW and CW voltages are translated into the dq reference frame. Note that the dq reference frame is aligned with the PW flux orientation

TABLE 1: Summary of literature review.

Features	[23]	[24]	[25]	[26]	[27]	[28]	[29]	Proposed
Grid-connected				✓		✓	✓	✓
DC-link control	✓	✓	✓		✓	✓	✓	✓
Rotor-side converter control	✓				✓			✓
Point-of-common-coupling voltage stabilization	✓	✓	✓			✓	✓	✓
Harmonic mitigation		✓		✓		✓		✓
Power control								✓
IMC PI regulators								✓

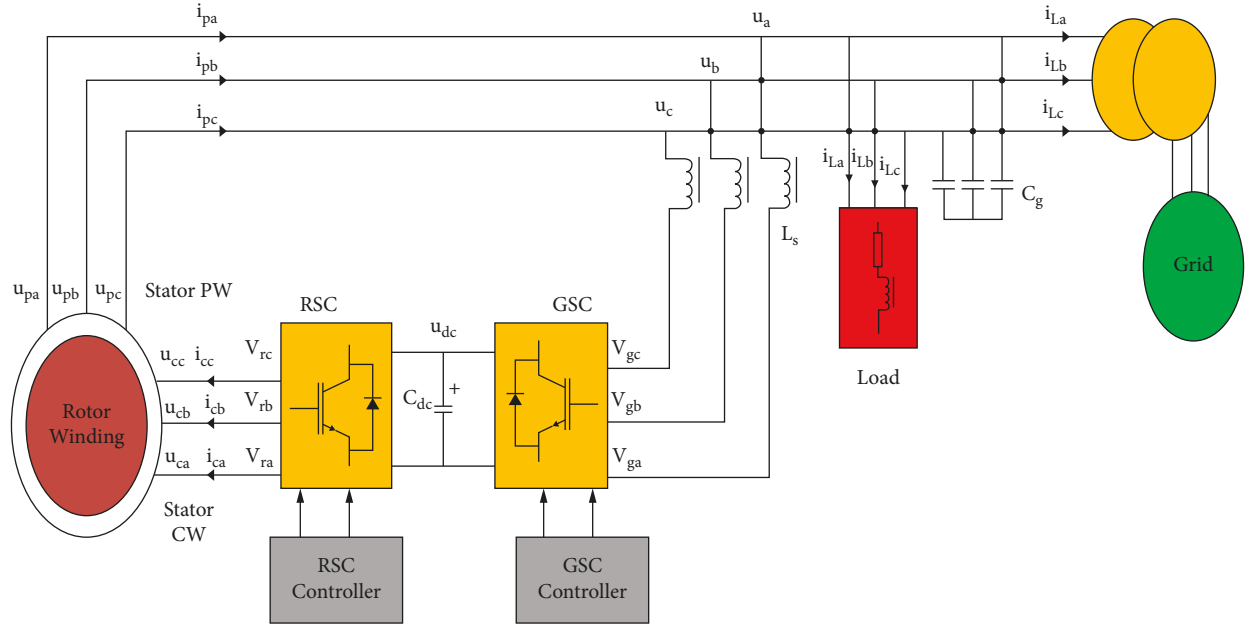


FIGURE 1: System model.

[30,31]. The resulting dq components for PW are given as follows:

$$u_{pd} = i_{pd}R_p - j\omega_p\lambda_{pq} + \frac{d\lambda_{pd}}{dt}, \quad (1)$$

$$u_{pq} = i_{pq}R_p + j\omega_p\lambda_{pd} + \frac{d\lambda_{pq}}{dt}, \quad (2)$$

$$\lambda_{pd} = L_p i_{pd} + L_r i_{rd}, \quad (3)$$

$$\lambda_{pq} = L_p i_{pq} + L_r i_{rq}, \quad (4)$$

where u_{pd} and u_{pq} denote the d and q components of PW voltage, while λ_{pd} and λ_{pq} symbolize the d and q components of PW flux. Similarly, the d and q components for CW are depicted as follows:

$$u_{cd} = i_c R_c - j(\omega_p - N_r \omega_r) \lambda_{cq} + \frac{d\lambda_{cd}}{dt}, \quad (5)$$

$$u_{cq} = i_c R_c + j(\omega_p - N_r \omega_r) \lambda_{cd} + \frac{d\lambda_{cq}}{dt}, \quad (6)$$

$$\lambda_{cd} = L_c i_{cd} + L_{rc} i_{rd}, \quad (7)$$

$$\lambda_{cq} = L_c i_{cq} + L_{rc} i_{rq}, \quad (8)$$

where u_{cd} and u_{cq} denote the d and q components of CW voltage, while λ_{cd} and λ_{cq} show the d and q components of CW flux. Similarly, for the d and q components for the rotor, given rotor current i_r is given as

$$u_{rd} = 0 = i_{rd} R_r - j(\omega_p - P_p \omega_r) \lambda_{rq} + \frac{d\lambda_{rd}}{dt}, \quad (9)$$

$$u_{rq} = 0 = i_{rq} R_r - j(\omega_p - P_p \omega_r) \lambda_{rd} + \frac{d\lambda_{rq}}{dt}, \quad (10)$$

$$\lambda_{rd} = L_r i_{pd} + L_{rc} i_{cd} + L_r i_{rd}, \quad (11)$$

$$\lambda_{rq} = L_r i_{pq} + L_{rc} i_{cq} + L_r i_{rq}, \quad (12)$$

where u_{rd} and u_{rq} denote the d and q components of rotor voltage, while λ_{rd} and λ_{rq} represent the d and q components of rotor flux. Finally, the rotor torque can be calculated as follows:

$$T_e = -\frac{3}{2} P_p I_m [\lambda_p^* i_p] - \frac{3}{2} P_c I_m [\lambda_c^* i_c]. \quad (13)$$

TABLE 2: Table of notations.

Notation	Description
u_{pa}, u_{pb}, u_{pc}	Stator PW voltage
u_{ca}, u_{cb}, u_{cc}	Stator CW voltage
u_a, u_b, u_c	Stator PW voltage at PCC
u_{dc}	DC-link voltage
v_{ra}, v_{rb}, v_{rc}	RSC voltage
v_{ga}, v_{gb}, v_{gc}	GSC voltage
i_{pa}, i_{pb}, i_{pc}	Stator PW current
i_{ca}, i_{cb}, i_{cc}	Stator CW current
i_{La}, i_{Lb}, i_{Lc}	Load current
i_{Ta}, i_{Tb}, i_{Tc}	Grid current
C_{dc}	DC-link capacitor
C_g	Capacitor bank
L_s, L_L	Filter and load inductance
R_s, R_L	Internal and load resistance
R_p, R_c, R_r	Stator power winding, control winding, and rotor resistance
L_p, L_c, L_r	Stator power winding, control winding, and rotor leakage inductance
L_{pm}, L_{cm}	Magnetizing inductance of power winding/control winding
L_{rpm}, L_{rcm}	Magnetizing inductance of rotor to power winding/control winding

The VC scheme is designed for both RSC and GSC based on the preceding analytical model for the BDFIG-based wind turbine. Its purpose is to regulate the machine parameters at no load condition with the improved dynamic response. This is achieved by selecting the PI regulators' gains by the IMC method. The notations set for this paper is listed in Table 2.

3. Proposed RSC-Based Vector Control

This section presents the technique that has been proposed to improve the transient behavior when using a BDFIG. By employing a vector controller oriented on the frame of PW reference, a method has been proposed to control both active and reactive power independently. To determine the active power and reactive power analytically, the BDFIM mathematical model is used, while the IMC method is used to calculate the PI controller gains. In the vector control scheme, the reactive power and speed of the machine are controlled by regulating the dq components of the PW and CW currents. Figure 2 shows the controllers for the converters, namely, RSC and GSC. The per-phase steady-state equivalent circuit of a BDFIG is shown in Figure 3 [23, 28]. Using the DC capacitance (C_{dc}), the RSC and GSC are decoupled.

3.1. IMC-Based Rotor-Side Converter. The link between CW and RSC controls active and reactive powers across both by utilizing the d and q components, respectively. As a result of combining the mathematical expressions with the governing equations, a nonlinear dynamic model for the BDFIG can be derived, illustrating the affiliation between both stator windings, which is governed by the cross-coupling between

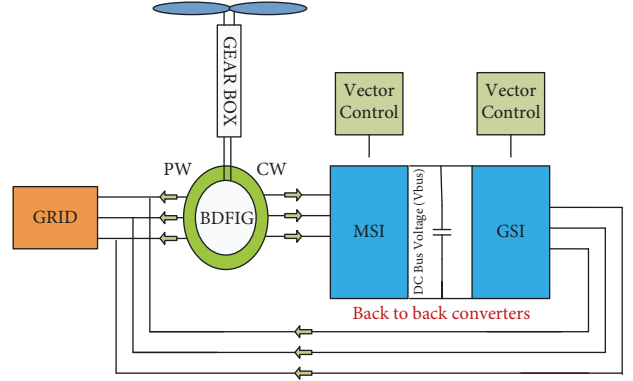


FIGURE 2: BDFIG with the VC scheme.

them. First, the CW current dq components are given as follows [32, 33]:

$$i_{cd} = \beta_1 i_{pd} + \beta_2 \frac{di_{pd}}{dt} - \beta_3 \lambda_p - \beta_4 \frac{d\lambda_{pd}}{dx} - j\omega_p \beta_4 \omega_p \lambda_{pd} + j\omega_p \beta_2 i_{pq} - j\omega_p i_{cq}, \quad (14)$$

$$i_{cq} = \beta_1 i_{pq} + \beta_2 \frac{di_{pq}}{dt} - \beta_3 \lambda_p - \beta_4 \frac{d\lambda_{pq}}{dx} - j\omega_p \beta_5 \lambda_{pq} + j\omega_p \beta_2 i_{pd} - j\omega_p i_{cd}, \quad (15)$$

where β_1 , β_2 , β_3 , and β_4 symbolize the control for PW current coefficients of open loop. Thus, transfer function can now be obtained for the CW current as follows:

$$i_c = \beta_1 i_p + \beta_2 \frac{di_p}{dt}. \quad (16)$$

Using a similar approach as above, we can derive the CW voltage, i.e., regulating CW voltage using the CW current [27]:

$$u_{cd} = \alpha_1 i_{cd} + \alpha_2 \frac{di_{cd}}{dt} + (-\alpha_3 + j\alpha_4) \lambda_{pd} + \alpha_5 \frac{d\lambda_{pd}}{dx} + (\alpha_6 + j\alpha_7) i_{pq} - j\alpha_8 i_{cq}, \quad (17)$$

$$u_{cq} = \alpha_1 i_{cq} + \alpha_2 \frac{di_{cq}}{dt} + (-\alpha_3 + j\alpha_4) \lambda_{pq} + \alpha_5 \frac{d\lambda_{pq}}{dx} + (\alpha_6 + j\alpha_7) i_{pd} - j\alpha_8 i_{cd}, \quad (18)$$

where $\alpha_1, \alpha_1, \dots, \alpha_5$ represents the control for CW current coefficients of open loop. Thus, the transfer function for CW voltage is given by

$$u_c = \alpha_1 i_c + \alpha_2 \frac{di_c}{dt}. \quad (19)$$

This is the mathematical model of the system with respect to voltage and current. The feed-forward compensation has been used to deal with external disturbances as it is one of the most common methods to handle them [15]. A

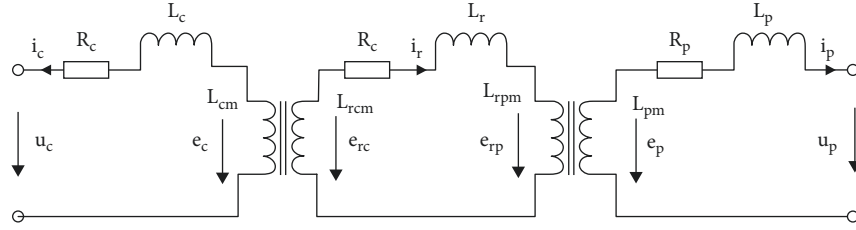


FIGURE 3: BDFIG equivalent circuit.

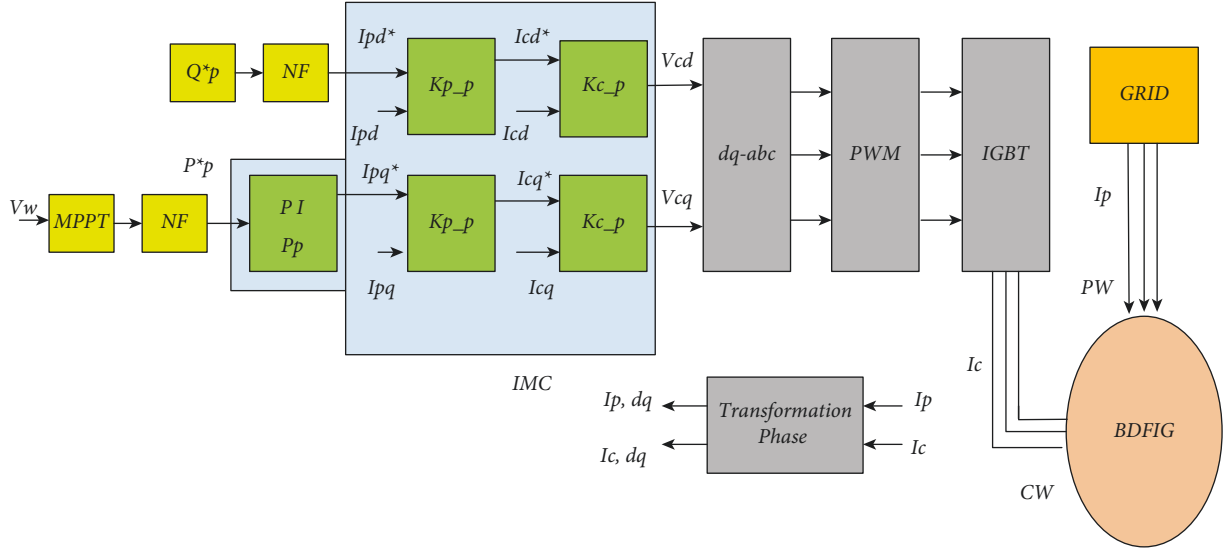


FIGURE 4: Rotor-side converter with the VC scheme.

method of capturing external disturbances and improving the stability of systems based on IMC is proposed in this paper. The proposed RSC using the IMC method with a notch filter is shown in Figure 4.

The standard IMC structure as given in [34] has been used to extract the PI gains.

$$F_s = \begin{bmatrix} K_p + \frac{K_i}{s} & 0 \\ 0 & K_p + \frac{K_i}{s} \end{bmatrix}. \quad (20)$$

In terms of the gain values suggested by this IMC approach, the following expressions have been used:

$$K_p^{PW} = 2\pi B_p \beta_2, \quad (21)$$

$$K_i^{PW} = 2\pi B_p \beta_1, \quad (22)$$

$$K_p^{CW} = 2\pi B_c \alpha_2, \quad (23)$$

$$K_i^{CW} = 2\pi B_c \alpha_1, \quad (24)$$

where K_p^{PW} , K_i^{PW} and K_p^{CW} , K_i^{CW} denote the gain values for PW and CW current, respectively. Similarly, B_p and B_c represent the frequency bandwidth for PW and CW, respectively.

3.2. Control of Active and Reactive Power. After selecting the PI gains through the IMC method, the methodology for controlling active and reactive power with NF is obtained from the single-phase equivalent circuit for the stand-alone BDFIG system, as shown in Figure 5. In Figure 5, i_{L1} is the a-phase load current for a-phase, u_a and i_a are the a-phase voltage and current at the PCC. Symbolizing the amplitude-frequency by U_m and angular frequency of the phase voltage ω , respectively, e_{pa} can be obtained as follows [23]:

$$e_{pa}(t) = U_m \cos(\omega t). \quad (25)$$

Converting equation (25) into the Laplace transform of, e_{pa} can be obtained in the complex frequency domain as follows:

$$e_{pa}(s) = U_m s \left(\frac{U_m s}{s^2 + \omega^2} \right). \quad (26)$$

Under normal conditions and at a natural speed $i_a = 0$, it can be assumed that the grid line resistance is negligible, and this assumption should be made without loss of generality. It is also important to note that when the load is attached, the switch will be closed, which will force the current into the stator as [23]

$$i_{pa}(s) = U_m s \left(\frac{e_{ca}(s)}{L_s + R} \right) = \frac{U_m}{(L_s + R)(s^2 + \omega^2)}, \quad (27)$$

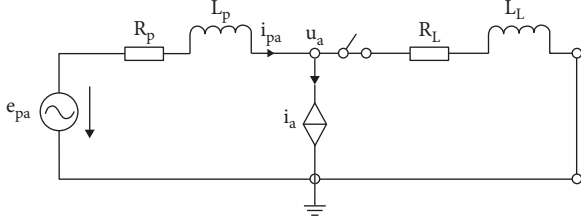


FIGURE 5: Single-phase equivalent circuit from PW.

where L shows the total inductance and total resistance is indicated by R are given by

$$R = R_c + R_l + R_s, \quad (28)$$

$$L = L_c + L_l + L_L. \quad (29)$$

It is necessary to define the magnitude and the angle of the total impedance in the following manner:

$$|Z| = \sqrt{R^2 + (\omega L)^2}, \quad (30)$$

$$\Phi = \arctan\left(\frac{\omega L}{R}\right). \quad (31)$$

Equation (27) can be rewritten as [23]

$$i_{pa}(s) = \frac{U}{|Z|^2} \left(\frac{R_s}{(s^2 + \omega^2)} + \frac{\omega^2 L}{(s^2 + \omega^2)} - \frac{RL}{L_s + R} \right), \quad (32)$$

$$i_{pa}(s) = \frac{U}{|Z|} \left(\frac{s \cos \Phi}{(s^2 + \omega^2)} + \frac{\omega \sin \Phi}{(s^2 + \omega^2)} - \frac{\cos \Phi}{L_s + R} \right). \quad (33)$$

Converting into the inverse Laplace transform, we get

$$i_{pa}(s) = \frac{U}{|Z|} (\cos(\omega t - \Phi)) - \frac{U}{|Z|} (\cos(-\Phi) e^{-(R/L)t}). \quad (34)$$

In equation (34), it shows that the current of the PW consists of two components. A fundamental frequency component is the first of the two components, and the second is an exponentially decaying DC component. On the same principle, equations can be provided for the current in both the b and c phases of the stator PW. Consequently, active and reactive power for both the fundamental frequency and exponentially decaying DC component of the machine is given as

$$P_{pa}(s) = e_{pa}(s) i_{pa}(s) \cos(\Phi), \quad (35)$$

$$Q_{pa}(s) = e_{pa}(s) i_{pa}(s) \sin(\Phi). \quad (36)$$

The use of the above equations for power in the simulation will achieve the appropriate control within the vector control strategy. We observe a harmonic component at twice high of frequency despite this. Wang et al. in reference [23] made an attempt to avoid this component and also proposed the instantaneous reactive power (IRP) theory, which increases the complexity and results in suboptimal performance. The use of a notch filter has been proposed to

TABLE 3: Parameter of the 2nd-order notch filter.

Parameter	Symbol	Units	Value
Center frequency	f_0	Hz	100
Sampling rate	f_s	Hz	1000
3 dB bandwidth	BW	Hz	2

eliminate the double fundamental frequency component in the voltage at the PCC following the reactive current compensation by the RSC. The notch filter has been used successfully in order to suppress harmonics.

3.3. Notch Filter Design. In its default configuration, a notch filter (NF) allows only frequencies in a narrow band and rejects frequencies outside of it. In addition to their conventional applications as band reject or band-stop filters, NFs may also be employed as prefilters to reject harmonics that feedback controllers do not eliminate. This type of rejection is needed to improve the system's response time or improve the bandwidth. The nonlinearities coming from switched components and their unpredictable functioning are a challenge when designing for complex systems. Upon finding the lightly damped mode, the complex pair of poles that cause the harmonics are derived from a linearized system. A complex pair of zeros with slightly higher damping must be placed first in the s -plane, followed by one with a slightly lower natural frequency. Doing so will ensure that the root-locus stays out of the right half of the plane [21]. Following the design guidelines of [24], we exploit a second-order band-stop digital NF with a transfer function that is as follows:

$$H(z) = K \frac{z^2 - 2z \cos \theta + 1}{z^2 - 2rz \cos \theta + r^2}, \quad (37)$$

$$\theta = \frac{f_0}{f_s},$$

$$r \approx 1 - \left(\frac{BW}{f_s}\right)\pi, \quad (38)$$

$$K = \frac{1 - 2r \cos \theta + r^2}{2 - 2 \cos \theta}.$$

Here, f_0 is the center frequency and BW is the 3 dB bandwidth. The NF parameters are given in Table 3.

The notch filter utilized in the GSC is shown in Figure 6.

The block diagram implementation of an NF with the parameters in Table 3 and equation (24) is shown in Figure 6.

One such NF is included as a prefilter for each phase as indicated by blocks labeled NF in Figure 7. An illustration of the frequency response of the NF can be seen in Figure 8.

The successful rejection of the unwanted frequency can be attributed to the high-quality factor $Q = f_0/BW = 50$.

4. Results and Discussion

The results to assess the effectiveness of the proposed controller are presented in this section. One of the contributions of current research work is that it has developed a

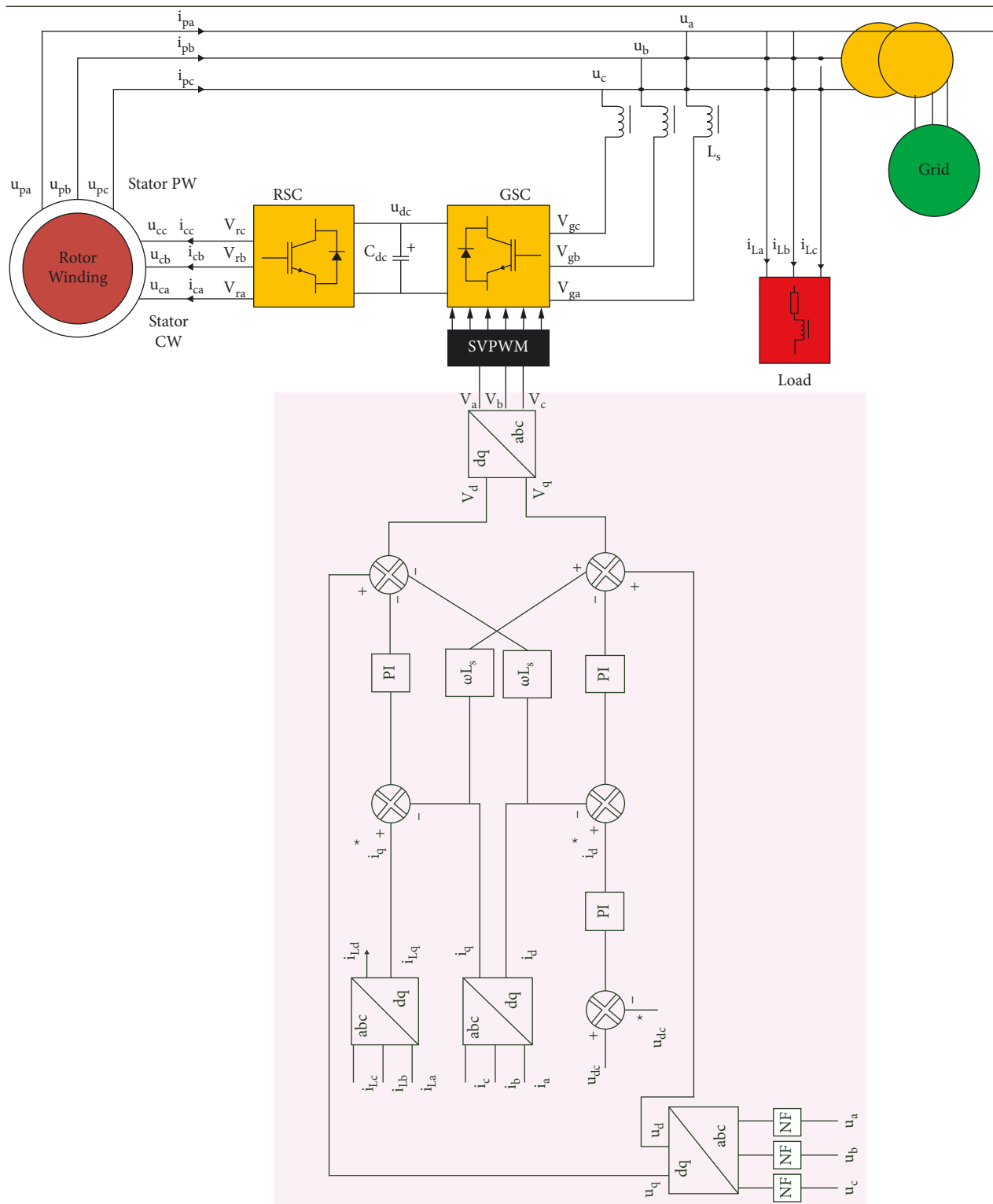


FIGURE 6: Proposed GSC controller with the notch filter.

BDFIG machine model connected with a wind turbine. The simulation parameters for the developed BDFIG machine model are provided in Table 4. A wind turbine model is considered constant with maximum power point tracking (MPPT) control that causes an increase in its power with a corresponding increase in wind speed. MPPT is used to

extract the maximum available power from the wind energy, which is then served as the reference active power to be attained from the considered BDFIG-based wind turbine. The wind speed V_w is considered constant (12m/s) throughout the simulation run. In order to control the BDFIG's generator, the VC scheme is simulated along with

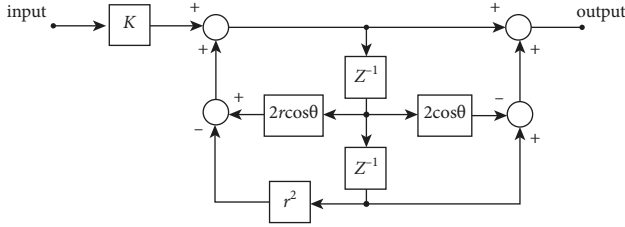


FIGURE 7: NF: block diagram.

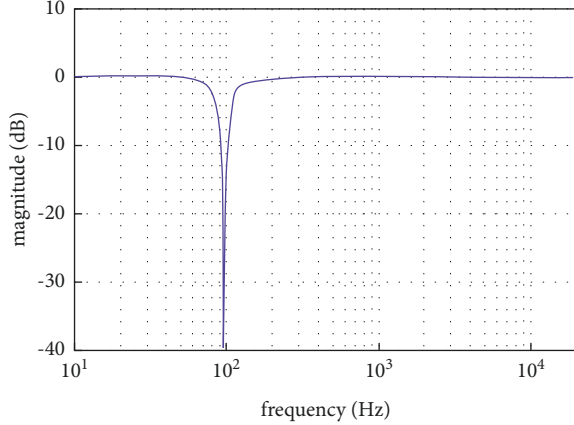


FIGURE 8: NF: frequency response.

TABLE 4: Simulation parameters.

Parameter	Value
MATLAB/Simulink version	R2020b
Simulation type	Discrete
Solver	Variable step ode23tb (stiff/TR-BDF2)
Sample time	5–10 s
Switching frequency	4 kHz
Rated stator power winding voltage	120 V
Rated stator power winding current	150 A
Rated operating frequency	50 Hz
Power factor	0.8
P_p, P_c	2, 6
ω_n	475 rpm
C_{dc}, u_{dc}	0.01 F, 700 V
L_s, L_p, L_c, L_r	0.214, 0.0715., 0.0122, 0.0133 p.u.
R_p, R_c, R_r	0.017, 0.0108, 0.047 p.u.
L_{rp}, L_{rc}	19.223, 5.035 p.u.

its RSC and GSC controls under inductive load conditions. Besides, the PI gains for controllers are calculated using the IMC method. The active power and volt-ampere reactive (VAR) controllers receive the error signals of P_1 and Q_1 to output v_{cd} and v_{cq} . The dq components of PW and CW current components are regulated to obtain the desired active and reactive powers. The signals to the PWM generator are being applied by the CW reference voltage after transforming dq components into three-phase components.

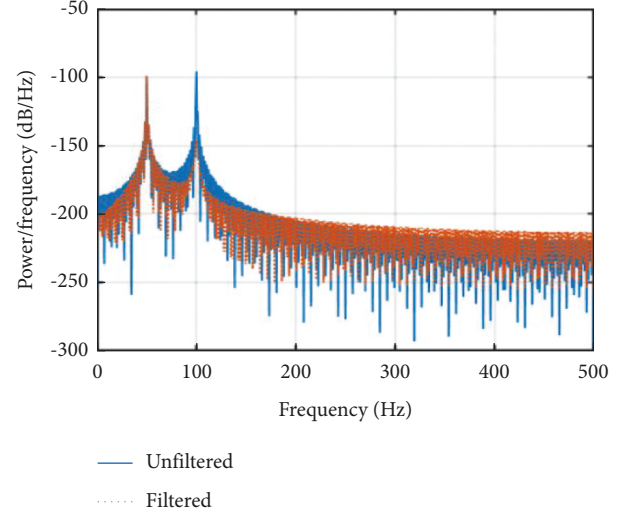


FIGURE 9: Power spectrum of voltage drop.

The PWM will generate a signal to switch the universal bridge, and CW will be supplied with a variable supply frequency, as shown in Figure 4.

A VC scheme is based on inner and outer control loops that can be implemented according to PI regulators. In terms of performance, the choice of the gains for these regulators plays an important role. It is commonly referred to use the “Ziedergger method” to choose these gains [35]. In this case, the WECS could undergo a large overshoot followed by a long settling period. The IMC technique is used in this paper to tune the PI regulators in order to adjust the BDFIG’s dynamic response to a desirable level.

Thus, we compared the performance of the proposed technique with the technique such as Ziegler method-based PI regulators gains with the addition of reactive power theory to remove the harmonics that increase the system’s complexity due to the involvement of the transformation method. Thus, the system cannot reject the narrowband frequency, which ultimately results in suboptimal performance. The frequency response of the voltage drops with NF and reactive power theory is plotted in Figure 9. A double fundamental frequency harmonic is observed without any filtering. However, the double frequency harmonic has been compensated significantly using the proposed NF. It can be observed that the NF reduces the double fundamental frequency harmonic significantly to near rejection.

To assess the performance of the proposed technique, inductive load with three different reactive power levels, 30, 45, and 55 kVARs, is considered. The load’s active power is set at 4.5 KW, and the inductive load is allowed to connect at 3 ms. The objective is to control active and reactive power with a less transient response while eliminating the double frequency harmonic using the notch filter. It is observed that the proposed technique-based controller significantly reduced the transients in both active and reactive powers. The comparison shows that the proposed technique outperformed the existing method, as it attained machine parameters such as PW voltage, CW current, PW current, machine speed, and active and reactive power far better than

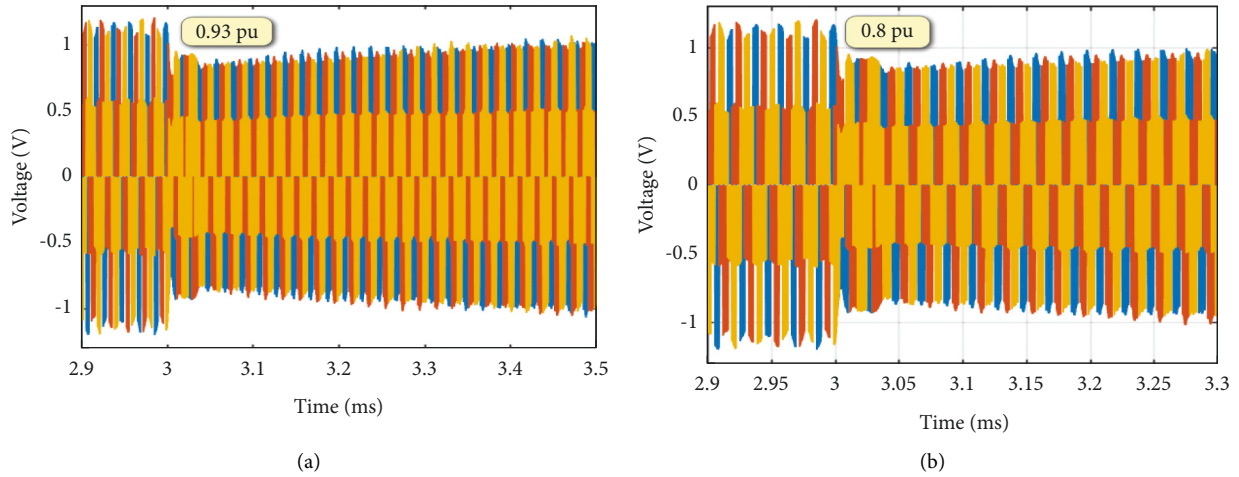


FIGURE 10: PW voltage. (a) Voltage with the proposed technique. (b) Voltage with technique 1.

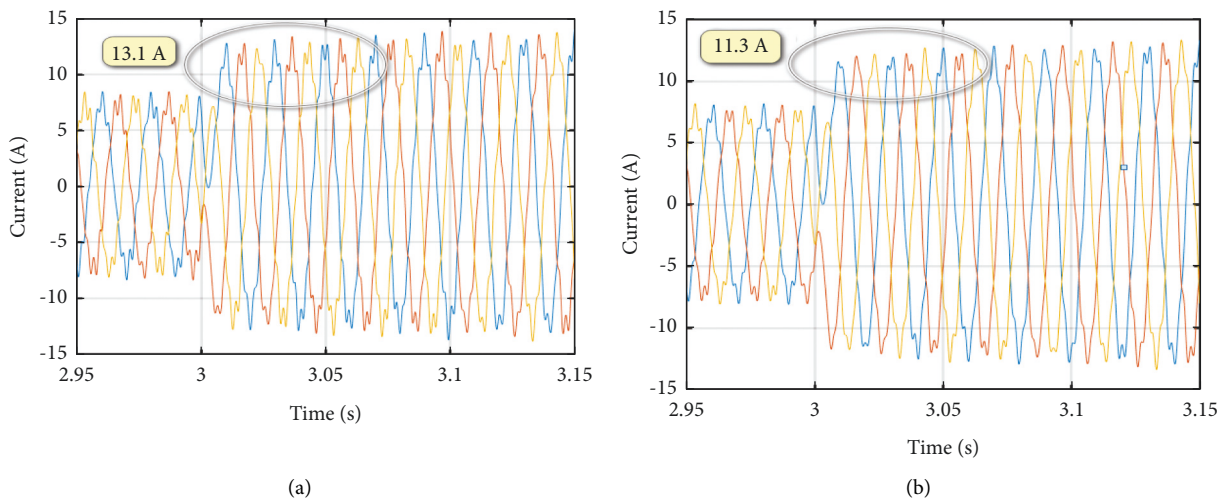


FIGURE 11: CW current. (a) Control winding current—proposed technique. (b) Control winding current—technique 1.

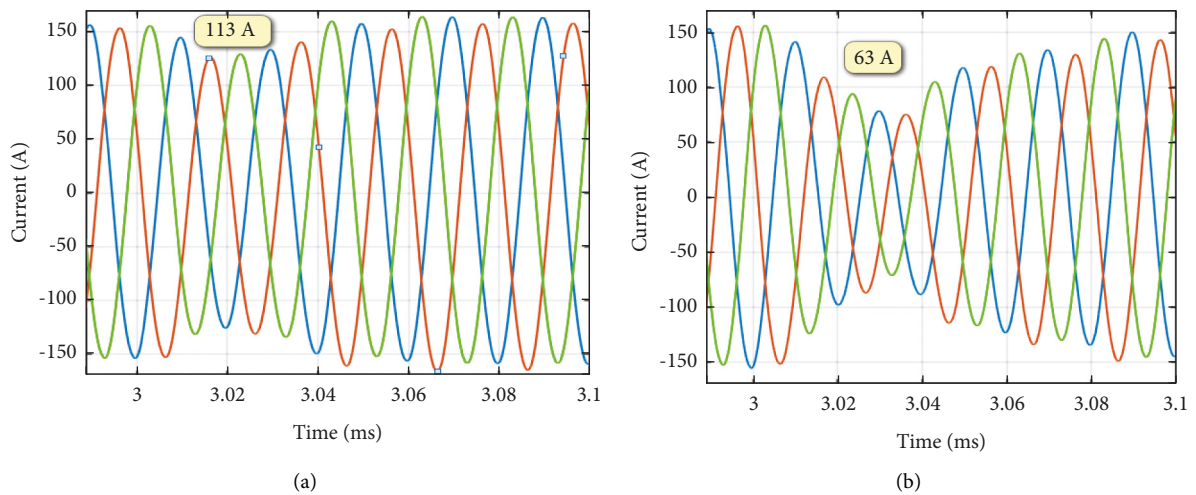


FIGURE 12: PW current. (a) Power winding current—proposed technique. (b) Power winding current—technique 1.

TABLE 5: Control of machine parameters comparison.

	Proposed technique	Technique 1	Improvement
PW voltage (p.u)	0.8	0.93	0.13
CW current (A)	13.1	11.3	1.8
PW current (A)	113	63	50

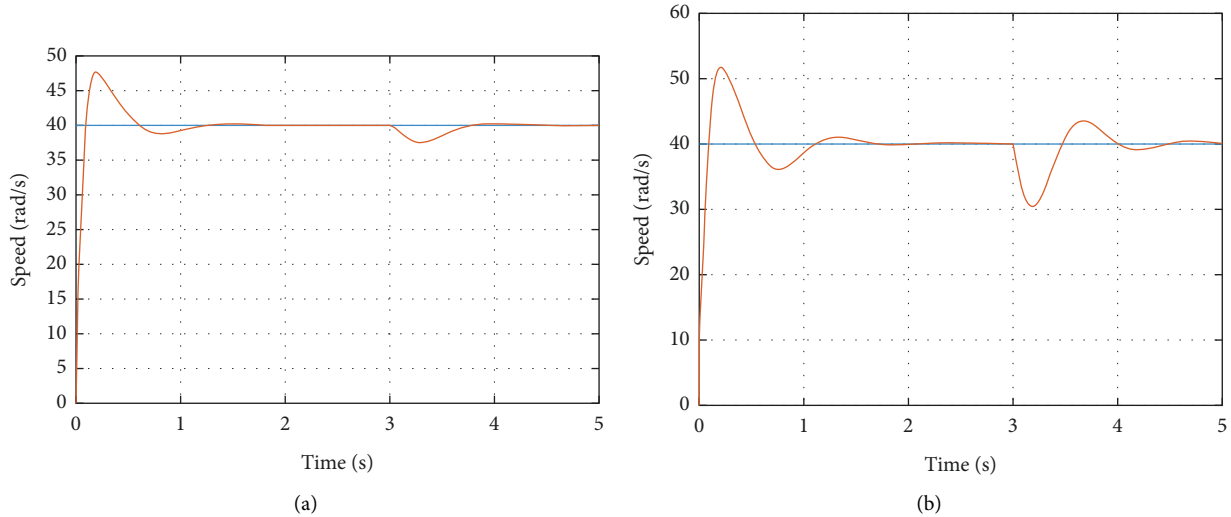


FIGURE 13: Speed control. (a) Speed—proposed technique. (b) Speed—technique 1.

TABLE 6: Speed control comparison.

	Max: Peak (rad/s)	Min: Peak (rad/s) (at 3 sec)	Settling time (s)
	Speed (r/s)		
Proposed technique	47.4	38.2	1.3
Technique 1	51.69	30.4	1.8

the present levels. Besides, it is also observed that the IMC-based PI tuning improves the dynamic response while the notch filter significantly reduces the double fundamental frequency harmonic. The PW voltage's response with and without the proposed technique is shown in Figure 10.

Note: The proposed technique employs IMC-based PI gains calculations with a notch filter design, whereas the technique 1 uses Ziegler method-based PI regulators gains with the addition of reactive power theory.

Figure 10 shows that the PW voltage is reduced to 0.8 pu with the IRP method, which may cause the disconnection of load. However, the PW voltage remains close to 1 p.u with the proposed method when the inductive load having 30 KVAR is added to the grid-connected system. It has already been mentioned that the machine has a control winding current that must be sufficient to control the converter. The technique used in this paper successfully maintains a 13.1 A current compared to the CW's 11.3 A current; see Figure 11(a).

The PW is connected directly to the grid through the PCC; it should remain close to its rated value when the inductive load is inserted into the system. The PW will be

close to the cut-off value, which increases the chances of load disconnection if the proper control system is not provided. Figure 12(a) shows that the proposed control technique reduced the PW current by 113 A compared to the most recent technique's 63 A.

The improved results obtained for PW voltage, CW current, and PW current with the proposed technique are shown in Table 5. The speed of the machine plays an important role in determining the machine's performance. The electrical machines in WECS need to provide consistent power output despite the continuous variations in wind speed. The wind speed decides the amount of power that can be extracted from WECS. In this way, it leads to generating a frequency with variable characters. This situation becomes problematic when the wind turbines are connected to a synchronized frequency grid system. The connection of variable frequency with fixed grid frequency raises the issues of power flickering, unstable situations, and system disconnection. Hence, the machine speed maintains its value even if an inductive load is inserted with less transients and overshoot, as shown in Figure 13(a) with the proposed control technique. However, the speed is found to have more

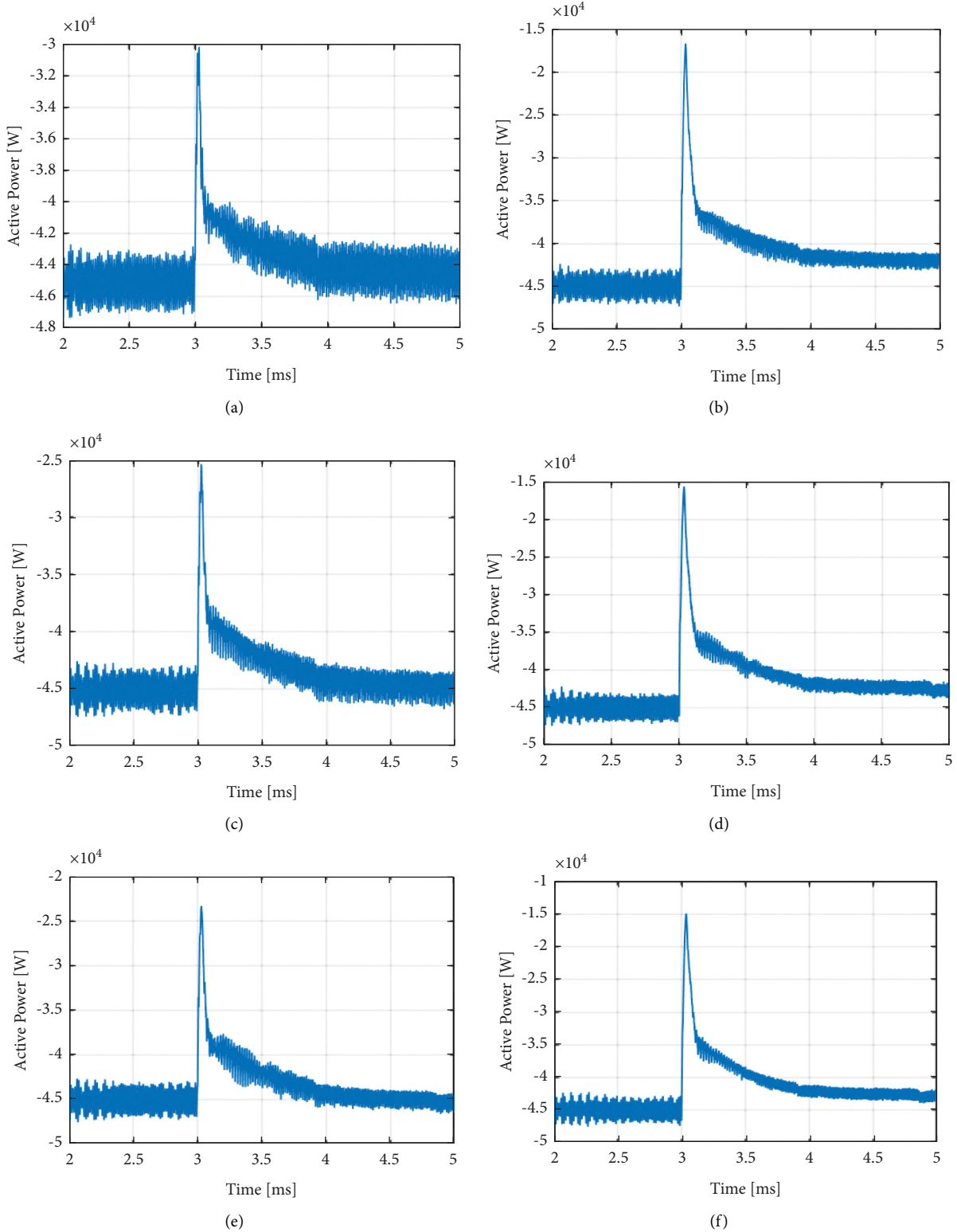


FIGURE 14: Comparison of the proposed technique with technique 1—active power. (a) $Q_L = 30$ KVAR—proposed technique. (b) $Q_L = 30$ KVAR—technique 1. (c) $Q_L = 45$ KVAR—proposed technique. (d) $Q_L = 45$ KVAR—technique 1. (e) $Q_L = 55$ KVAR—proposed technique. (f) $Q_L = 55$ KVAR—technique 1.

overshoots at the machine starting and load insertion instants. It proves the superiority of the proposed technique over the existing method.

Table 6 shows that the speed control with the proposed technique produces satisfactory results compared with technique 1 in terms of maximum peak, minimum peak, and

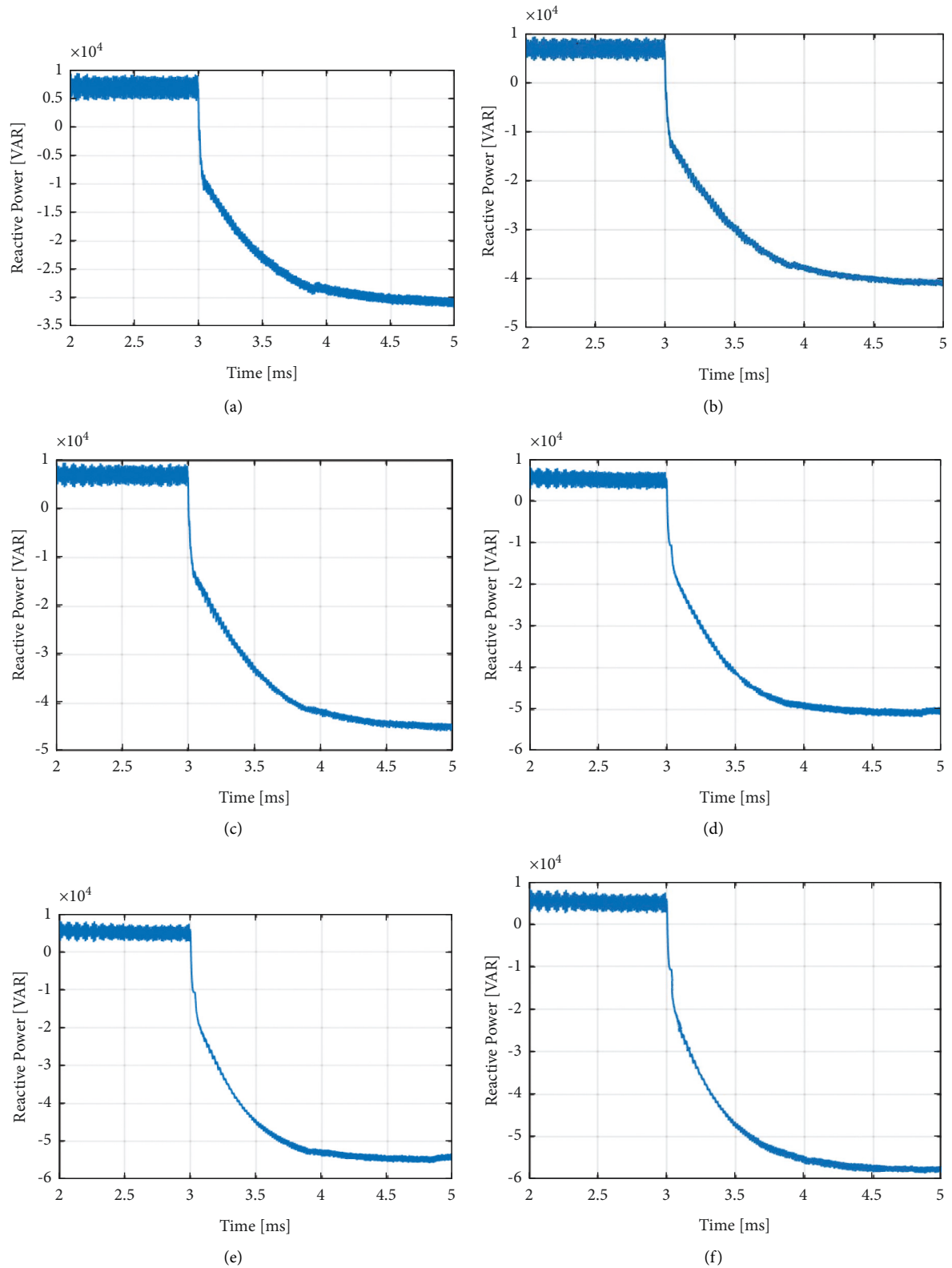


FIGURE 15: Comparison of the proposed technique with technique 1—reactive power. (a) $Q_L = 30$ KVAR—proposed technique. (b) $Q_L = 30$ KVAR—technique 1. (c) $Q_L = 45$ KVAR—proposed technique 1. (d) $Q_L = 45$ KVAR—technique 1. (e) $Q_L = 55$ KVAR—proposed technique. (f) $Q_L = 55$ KVAR—technique 1.

TABLE 7: Peak value comparison.

Q_L	Technique 1	Proposed technique
<i>Peak value (active power)</i>		
30	-1.69	-3.02
45	-1.55	-2.57
55	-1.50	-2.35
<i>Peak value (reactive power)</i>		
30	-4.63	-3.12
45	-5.09	-4.52
55	-5.48	-5.09

settling time. Active and reactive power control at the instant of multilevel inductive load integration is crucial since it contributes to the smooth electrical power supply. Although the active power is set at 4.5 kW, a comparison with the IRP technique may be seen in terms of the controller's transient response and ability to revert to its original value when the reactive power of the load is altered, shown in Figure 14. Likewise, the reactive power values such as 30 kVAr, 45 kVAr, and 55 kVAr are also seen in Figure 15 and compared with the IRP technique.

The active power and reactive power for three types of loads are shown in Figures 14 and 15, along with the comparison with technique 1. The proposed technique appears to control the active and reactive power with better dynamic ability when inductive loads add to the BDFIG system. This is evident from its performance in regulating BDFIG's power. Adding a notch filter removes the double fundamental harmonics that further improves the power system. Compared with that particular technique 1, the results obtained with the proposed work meet the expectations.

The improvements achieved by the proposed technique are delineated obviously in Table 7.

It can be seen that in all three cases, the proposed technique offers an improvement in the case of obtaining less peak value for the active and reactive power during inductive load insertion.

5. Conclusion

This paper presented a method for improving the transient behavior of a BDFIG's RSC when an inductive load is abruptly applied to the PCC. The IMC approach was used to calculate the PI gains for the BDFIG in order to help the machine improve its dynamic response. Based on the analysis of the voltage drop at the PCC using the power equations as a reference, a double fundamental frequency harmonic appears to exist, and a notch filter is designed to remove this double fundamental frequency harmonic. Simulations were performed in MATLAB/Simulink to evaluate the proposed controller thoroughly. The results suggest that the proposed technique can reduce the overshoot and the peak value while simultaneously controlling the active and reactive power.

Data Availability

No data were used to support this study.

Conflicts of Interest

The authors declare that they have no conflicts of interest.

References

- [1] M. Wassan, K. Habib, and S. Hassan, "Mathematical modelling and simulation of the dehumidifier for the tropical region of Malaysia," 2013, https://ieeexplore.ieee.org/abstract/document/6560245/?casa_token=BhfnCtRbAIgAAAAA:RnEZ_Ey5BisG1l6FFwp66hcrU2wDvEuCdtu0MP41e7IdPpo9xnyylz0KOusV5CGfbfhsBA4H.
- [2] M. A. Wassan, K. Habib, and S. Bin Hassan, "Mathematical modeling for the regenerator of liquid desiccant air-conditioning system," *Applied Mechanics and Materials*, vol. 465, pp. 226–231, 2014.
- [3] P. Han, M. Cheng, Y. Jiang, and Z. Chen, "Torque/power density optimization of a dual-stator brushless doubly-fed induction generator for wind power application," *IEEE Transactions on Industrial Electronics*, vol. 64, no. 12, pp. 9864–9875, 2017.
- [4] R. M. Monteiro Pereira, A. J. C. Pereira, C. M. Ferreira, and F. Barbosa, "Influence of crowbar and chopper protection on DFIG during low voltage ride through," *Energies*, vol. 11, no. 4, p. 885, 2018.
- [5] M. Gholizadeh, S. Tohidi, A. Oraee, and H. Oraee, "Appropriate crowbar protection for improvement of brushless DFIG LVRT during asymmetrical voltage dips," *International Journal of Electrical Power & Energy Systems*, vol. 95, pp. 1–10, 2018.
- [6] A. Khidrani, M. H. Habibuddin, M. W. Mustafa, M. N. Aman, and A. S. Mokhtar, "A hybrid voltage-current compensator using a synchronous reference frame technique for grid-connected microgrid under nonlinear load conditions," *International Transactions on Electrical Energy Systems*, vol. 30, no. 10, Article ID e12530, 2020.
- [7] S. Bayhan, P. Kakosimos, and M. Rivera, "Predictive torque control of brushless doubly fed induction generator fed by a matrix converter," 2018, <https://ieeexplore.ieee.org/abstract/document/8372497/>.
- [8] X. Wei, M. Cheng, R. Luo, L. Xu, and J. Zhu, "Model predictive virtual power control of brushless doubly-fed induction generator for fast and smooth grid synchronisation," *IET Renewable Power Generation*, vol. 13, no. 16, pp. 3080–3087, 2019.
- [9] A. Rahab, F. Senani, H. Benalla, and R. Abderezak, "Direct power control of brushless doubly-fed induction generator used in wind energy conversion system," *International Journal of Power Electronics and Drive Systems (IJPEDS)*, vol. 8, no. 1, p. 417, 2017.
- [10] R. Zhao, A. Zhang, Y. Ma, X. Wang, J. Yan, and Z. Ma, "The dynamic control of reactive power for the brushless doubly fed induction machine with indirect stator-quantities control scheme," *IEEE Transactions on Power Electronics*, vol. 30, no. 9, pp. 5046–5057, 2015.
- [11] T. Jumani, M. Mustafa, and N. Hamadneh, "Computational intelligence-based optimization methods for power quality and dynamic response enhancement of ac microgrids," 2020, <https://www.mdpi.com/790260>.
- [12] S. Altbawi, A. Mokhtar, T. Jumani, I. Khan, N. N. Hamadneh, and A. Khan, "Optimal design of fractional order PID controller based automatic voltage regulator system using gradient-based optimization algorithm," 2021, <https://www.sciencedirect.com/science/article/pii/S1018363921001082>.

- [13] A. Memon, M. W. B. Mustafa, T. A. Jumani, M. Olatunji Obalowu, and N. R. Malik, "Salp swarm algorithm-based optimal vector control scheme for dynamic response enhancement of brushless double-fed induction generator in a wind energy conversion system," *International Transactions on Electrical Energy Systems*, vol. 31, no. 12, Article ID e13157, 2021.
- [14] A. Memon, M. W. Mustafa, A. Khidrani, F. Hafeez, S. K. Baloach, and T. A. Jumani, "Internal mode control based coordinated controller for brushless doubly fed induction generator in wind turbines during fault conditions," *Indonesian Journal of Electrical Engineering and Computer Science*, vol. 23, no. 2, p. 650, 2021.
- [15] M. Su, W. Jin, G. Zhang, W. Tang, and F. Blaabjerg, "Internal model current control of brushless doubly fed induction machines," *Energies*, vol. 11, no. 7, p. 1883, 2018.
- [16] T. A. Jumani, M. W. Mustafa, M. M. Rasid, and Z. A. Memon, "Dynamic response enhancement of grid-tied ac microgrid using salp swarm optimization algorithm," *International Transactions on Electrical Energy Systems*, vol. 30, no. 5, Article ID e12321, 2020.
- [17] T. Jumani, M. Mustafa, and M. M. Rasid, "Optimal voltage and frequency control of an islanded microgrid using grasshopper optimization algorithm," 2018, <https://www.mdpi.com/367158>.
- [18] D. Muhammad Soomro, Z. A. Memon, M. A. Uqaili, and F. Abbasi, "Performance of shunt active power filter based on instantaneous reactive power control theory for single-phase system," *International Journal of Renewable Energy Research*, vol. 7, no. 4, 2017.
- [19] G. Gohil, L. Bede, R. Teodorescu, T. Kerekes, and F. Blaabjerg, "Line filter design of parallel interleaved VSCs for high-power wind energy conversion systems," *IEEE Transactions on Power Electronics*, vol. 30, no. 12, pp. 6775–6790, 2015.
- [20] R. Peña-Alzola, M. Liserre, F. Blaabjerg, M. Ordóñez, and Y. Yang, "LCL-filter design for robust active damping in grid-connected converters," *IEEE Transactions on Industrial Informatics*, vol. 10, no. 4, pp. 2192–2203, 2014.
- [21] M. Popescu, A. Bitoleanu, and V. Suru, "A DSP-based implementation of the $p-q$ theory in active power filtering under nonideal voltage conditions," *IEEE Transactions on Industrial Informatics*, vol. 9, no. 2, pp. 880–889, 2013.
- [22] R. Pavlanin and M. Marinelli, "Different view on pq theory used in the control algorithm of active power filters," 2011, <http://advances.vsb.cz/index.php/AEEE/article/view/183>.
- [23] X. Wang, H. Lin, and Z. Wang, "Transient control of the reactive current for the line-side converter of the brushless doubly-fed induction generator in stand-alone operation," *IEEE Transactions on Power Electronics*, vol. 32, no. 10, pp. 8193–8203, 2017.
- [24] W. Xu, K. Yu, Y. Liu, and J. Gao, "Improved coordinated control of standalone brushless doubly fed induction generator supplying nonlinear loads," *IEEE Transactions on Industrial Electronics*, vol. 66, no. 11, pp. 8382–8393, 2019.
- [25] Y. Liu, W. Xu, J. Zhu, and F. Blaabjerg, "Sensorless control of standalone brushless doubly fed induction generator feeding unbalanced loads in a ship shaft power generation system," *IEEE Transactions on Industrial Electronics*, vol. 66, no. 1, pp. 739–749, 2019.
- [26] Y. Liu, W. Xu, T. Long, and F. Blaabjerg, "An improved rotor speed observer for standalone brushless doubly-fed induction generator under unbalanced and nonlinear loads," *IEEE Transactions on Power Electronics*, vol. 35, no. 1, pp. 775–788, 2020.
- [27] J. Chen, W. Zhang, B. Chen, and Y. Ma, "Improved vector control of brushless doubly fed induction generator under unbalanced grid conditions for offshore wind power generation," *IEEE Transactions on Energy Conversion*, vol. 31, no. 1, pp. 293–302, 2016.
- [28] A. Memon, M. W. Mustafa, M. N. Aman, A. Hafeez, and M. Ullah, "Improving transient behavior of a brushless doubly fed induction generator through reactive current control of grid-side converter," *Electronics (Switzerland)*, vol. 10, p. 1413, 2021.
- [29] D. Low, A. Memon, M. W. Mustafa et al., "Dynamic low voltage ride through detection and mitigation in brushless doubly fed induction generators," *Energies*, vol. 14, 2021.
- [30] J. Poza, E. Oyarbide, D. Roye, and M. Rodriguez, "Unified reference frame dq model of the brushless doubly fed machine," *IEE Proceedings: Electric Power Applications*, vol. 153, no. 5, p. 726, 2006.
- [31] S. Shao, E. Abdi, F. Barati, and R. McMahon, "Stator-Flux-Oriented vector control for brushless doubly fed induction generator," *IEEE Transactions on Industrial Electronics*, vol. 56, no. 10, pp. 4220–4228, 2009.
- [32] J. Poza, E. Oyarbide, and D. Roye, "New vector control algorithm for brushless doubly-fed machines," *IEEE 2002 28th Annual Conference of the Industrial Electronics Society. IECON 02*, vol. 2, pp. 1138–1143, 2002.
- [33] J. Poza, E. Oyarbide, I. Sarasola, and M. Rodriguez, "Vector control design and experimental evaluation for the brushless doubly fed machine," *IET Electric Power Applications*, vol. 3, no. 4, p. 247, 2009.
- [34] L. Harnefors and H.-P. Nee, "Model-based current control of AC machines using the internal model control method," *IEEE Transactions on Industry Applications*, vol. 34, no. 1, pp. 133–141, 1998.
- [35] Z. Khan and J. J. Lehtomaki, "Interactive trial and error learning method for distributed channel bonding: model, prototype implementation, and evaluation," *IEEE Transactions on Cognitive Communications and Networking*, vol. 5, no. 2, pp. 206–223, Jun. 2019.